LANGMUIR

pubs.acs.org/Langmuir Article

Synthesis of Rough Colloidal SU-8 Rods and Bananas via Nanoprecipitation

Carla Fernández-Rico,* Jeffrey S. Urbach, and Roel P. A. Dullens*

Cite This: *Langmuir* 2021, 37, 2900−2906 Read Online

ACCESS | Metrics & More | Article Recommendations

ABSTRACT: Surface roughness plays an important role in determining the mechanical properties, wettability, and self-assembly in colloidal systems. In this work, we develop a simple and fast method to produce rough colloidal SU-8 rods, bananas, and spheres, via the nanoprecipitation of SU-8 in water. During this process, SU-8 nanospheres are absorbed onto the surface of the colloidal SU-8 particles and then cross-linked using UV-light. The size of the spherical asperities and the asperity density are controlled by the concentration of SU-8 used during the nanoprecipitation reaction. Fluorescent labeling of the rough SU-8 colloidal particles allows for their confocal imaging, which demonstrates their stability at high packing fractions. With these newly developed rough particles, we provide a colloidal model system that allows for studies addressing the impact of surface roughness on materials composed of anisotropic particles.

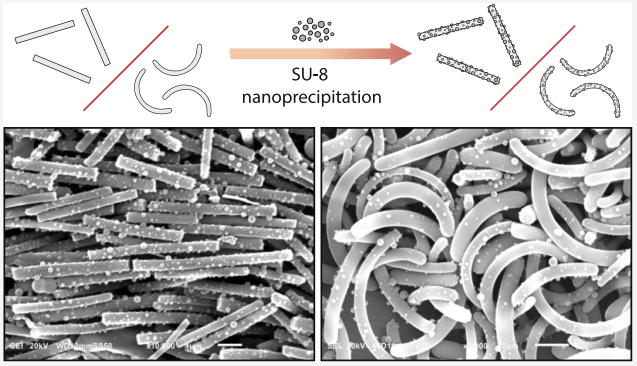

INTRODUCTION

Controlling the surface roughness of colloidal particles is a powerful tool for designing materials with engineered rheological, wetting, and self-assembly properties.[1] For instance, dense suspensions of rough colloidal spheres show shear thickening, i.e., a viscosity increase upon increasing shear rate, at lower shear rates than suspensions of colloidal spheres with a smooth surface.[2,3] This mechanical effect is explained in terms of interparticle frictional forces[3] and finds applications in shock-absorbing materials.[4] Surface roughness also plays an important role in the wetting behavior of colloidal particles at liquid−liquid interfaces.[5] This is particularly important for Pickering emulsions, in which droplets of water-in-oil (w/o) or oil-in-water (o/w) are stabilized by particles adsorbed at the oil−water interface. Interestingly, it has been shown that using rough particles, as opposed to smooth ones, increases the stability of Pickering emulsions[6] and also allows to stabilize o/w and w/o emulsions without changing their chemical properties.[5]

Another fascinating example of the impact of surface roughness at the colloidal scale is the directed self-assembly processes via depletion interactions.[7] The presence of surface asperities with a typical size larger than that of the depletant reduces the depletion attraction between particles[8] or parts of the particles,[7] leading, for example, to the selective formation of clusters depending on the particle roughness.[7] To date, most of the studies addressing the relationship between microscopic surface roughness and macroscopic properties of soft matter systems have been performed with colloidal spheres.[1,9] However, the impact of surface roughness on materials formed by anisotropic colloidal particles, and therefore the interplay between surface roughness and shape, remains unexplored due to the lack of rough anisotropic colloidal particles.

In this work, we develop a simple, fast, and scalable method to produce rough colloidal SU-8 rods and banana-shaped particles with tunable asperity size and asperity density. Using the nanoprecipitation of SU-8—a photoresist consisting of an epoxy-based oligomer, a solvent, and a photoacid initiator—we coat the surface of colloidal SU-8 particles[10,11] with SU-8 nanospheres. The resulting spherical asperities are subsequently cross-linked onto the SU-8 colloidal particles using UV-light exposure. We characterize the morphology of the resulting rough colloidal particles using scanning electron microscopy (SEM) and show that they form stable suspensions which can be imaged at the single-particle level with confocal microscopy. With our work, we provide a colloidal model system that can be used to address surface roughness-related phenomena in materials formed by anisotropic colloidal particles.

Received: November 23, 2020
Revised: January 25, 2021
Published: February 26, 2021

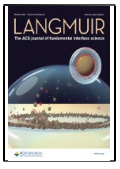

https://dx.doi.org/10.1021/acs.langmuir.0c03361
Langmuir 2021, 37, 2900−2906

EXPERIMENTAL SECTION

Materials. SU-8 50 (Microchem), γ-butyrolactone (GBL, ≥99%, Sigma-Aldrich), PEG-PPG-PEG pluronic F-108 (Sigma-Aldrich), and cyanine-3 fluorescent dye (Cy3, Lumiprobe) were used as received. Deionized water obtained directly from a purification system (Direct-Q 3 UV, Millipore) was used for all of the experiments.

Synthesis of "Bare" Colloidal SU-8 Particles. The syntheses of colloidal SU-8 rods, spheres, and bananas are described in[10] and.[11] The key steps of both procedures are briefly recapped here. For the synthesis of the colloidal SU-8 rods, approximately 0.1 g of SU-8 50 is injected into 110 mL of glycerol, which is subsequently mixed under high shear at 1500 rpm for 10 min. The resulting long SU-8 rods are then exposed to sonication (VWR ultrasonic cleaner, 45 kHz, 80 W) for 3 h to break them into smaller colloidal rods.[10] These rods are subsequently photo-crosslinked by exposing them to UV-light (365 nm, Spectroline 14A/FB) for 30 min. Finally, to remove the glycerol, the colloidal SU-8 rods are washed by repeated centrifugation and redispersion cycles using water containing 0.5 wt % Pluronic F-108.

For the synthesis of colloidal SU-8 spheres and bananas, the long SU-8 rods obtained after the high-shear mixing are heated, instead of sonicated, in a preheated oven at 95 °C for 30 min, which induces a shape deformation.[11] While colloidal SU-8 spheres are obtained when the rods are heated directly after their synthesis, the colloidal bananas are obtained when the rods are partially cross-linked with weak UV-light[11] during 25−45 min prior to the heating stage. After 30 min at 95 °C, the resulting SU-8 particles are fully cross-linked with strong UV-light exposure for 30 min and cleaned in a similar fashion as described for the colloidal SU-8 rods.

Synthesis of SU-8 Nanoparticles via Nanoprecipitation. SU-8 nanopsheres are produced via the nanoprecipitation of SU-8 in water. In a typical synthesis, 100 μL of a solution of SU-8 50 with concentrations ranging from 0.5 to 10 wt % SU-8 in GBL is added to 5 mL of water. After the addition of the SU-8 solution, SU-8 nanoparticles are immediately formed and the resulting dispersion is subsequently hand-shaken for 4−6 s. Next, 1 mL of Pluronic F-108 5 wt % in water is added to avoid coalescence of the formed spheres. The resulting SU-8 nanoparticles are then exposed to UV-light for 30 min and kept in water containing 1 wt % Pluronic F-108. For the synthesis of fluorescent SU-8 nanospheres, Cy3 (the fluorescent dye) was simply mixed with the SU-8 50 at a mass ratio of 10 mg dye/g SU-8 50.

Synthesis of Rough Colloidal SU-8 Particles. The synthesis of rough colloidal SU-8 particles is based on the adsorption of nanoprecipitated SU-8 nanospheres onto larger SU-8 colloidal particles via physisorption. To synthesize rough particles, we follow the same protocol as described in Synthesis of SU-8 Nanoparticles via Nanoprecipitation, but now the water phase contains colloidal SU-8 particles, i.e., rods, spheres, or bananas. In a typical reaction, the SU-8 particles are dispersed in 5 mL of pure water at an approximate particle concentration of 0.02 v/v%. Note that prior to this, the surfactant, which is typically present in particle suspensions in water, is removed via centrifugation and redispersion cycles in pure water. Next, we add 100 μL of a SU-8 solution with a concentration ranging from 0.5 to 10 wt % SU-8 50 in GBL to the aqueous dispersion of colloidal SU-8 particles. After hand-shaking the mixture for 4−6 s, 1 mL of 5 wt % Pluronics F-108 in water is added. The resulting dispersion is subsequently sonicated and vortexed for 10 s. The sample is subsequently UV-cured for 30 min to cross-link the SU-8 spherical asperities onto the surface of the colloidal particles. Finally, the bulk nanoparticles that did not adsorb onto the SU-8 colloidal particles are removed by means of centrifugation and redispersion cycles in water containing 1 wt % Pluronic F-108.

Scanning Electron Microscopy and Particle Dimensions. Scanning electron microscopy (SEM) images were taken with a JSM-6010LV electron microscope working at 15−20 kV. Samples were prepared by depositing a drop of diluted aqueous particle dispersion onto a 1 cm^2 silicon wafer. The solvent was evaporated using a heat lamp. Prior to the imaging, a thin layer of palladium was deposited on the sample using a Quorum sputter coater.

The size distributions of SU-8 nanoparticles and colloidal SU-8 particles were determined from SEM images by measuring the length and diameter of at least 400 particles using ImageJ and custom-written image analysis software in Mathematica. The dimensions of SU-8 asperities were determined by measuring the asperity diameter of at least 100 rough particles from SEM images using ImageJ. The polydispersity (%) of the particles is defined as $\sigma_i = \delta_i/\langle i \rangle$, where δ_i is the standard deviation and $\langle i \rangle$ the mean value.

Confocal Imaging of the Concentrated Samples of Rough Colloidal SU-8 Particles. For the confocal imaging of dense suspensions of rough colloidal SU-8 particles, we filled rectangular VitroCom capillaries (0.1 mm × 0.2 mm × 5 cm) with aqueous particle dispersions with an initial particle concentration of approximately 0.20 v/v% and subsequently sealed them using epoxy glue. After filling the sample cells, the colloidal particles slowly sedimented toward the bottom of the sample cell, where the imaging was performed. Confocal microscopy images with a 16 bit pixel depth were acquired using a 12 kHz resonant scanner head (Thorlabs) and a 532 nm laser, coupled to an Olympus IX73 inverted microscope equipped with a 60× (NA = 1.42) oil immersion objective (Olympus).

RESULTS AND DISCUSSION

In this work, we exploit the nanoprecipitation method to rapidly produce rough colloidal SU-8 particles (rods, spheres, and bananas) via the adsorption of SU-8 spheres onto the surface of the larger SU-8 colloidal particles. As an example, we show SEM images of the resulting rough SU-8 rods in Figure 1.

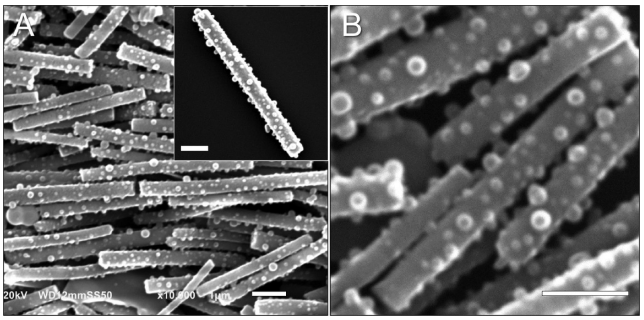

Figure 1. (A, B) Scanning electron microscopy images of rough SU-8 colloidal rods obtain via the nanoprecipitation of SU-8 in water. Scale bars are 1 μm.

We will describe our findings using rough colloidal SU-8 rods, but the same methods are used to fabricate rough colloidal SU-8 bananas and spheres. First, we will study the typical dimensions of the SU-8 nanospheres obtained via nanoprecipitation. Next, we will describe how nanoprecipitation is used to produce rough colloidal SU-8 particles with tunable asperity size and asperity density. Finally, we will present the confocal images of dense suspensions of rough rods and bananas and discuss their potential as colloidal model systems of rough anisotropic particles.

Synthesis of SU-8 Nanospheres via Nanoprecipitation. Nanoprecipitation is a simple and scalable method used for producing polymeric nanoparticles in an extremely fast fashion.[12−15] This method requires three main ingredients, a polymer, an organic solvent, and an aqueous solvent. The polymer is typically dissolved in the organic solvent, resulting in a polymer solution. It is essential that the organic and aqueous solvents are miscible with each other and that the polymer is insoluble in water. When these prerequisites are satisfied, the mixing of the polymer solution and the aqueous phase results in the instantaneous formation of polymer

https://dx.doi.org/10.1021/acs.langmuir.0c03361
Langmuir 2021, 37, 2900−2906

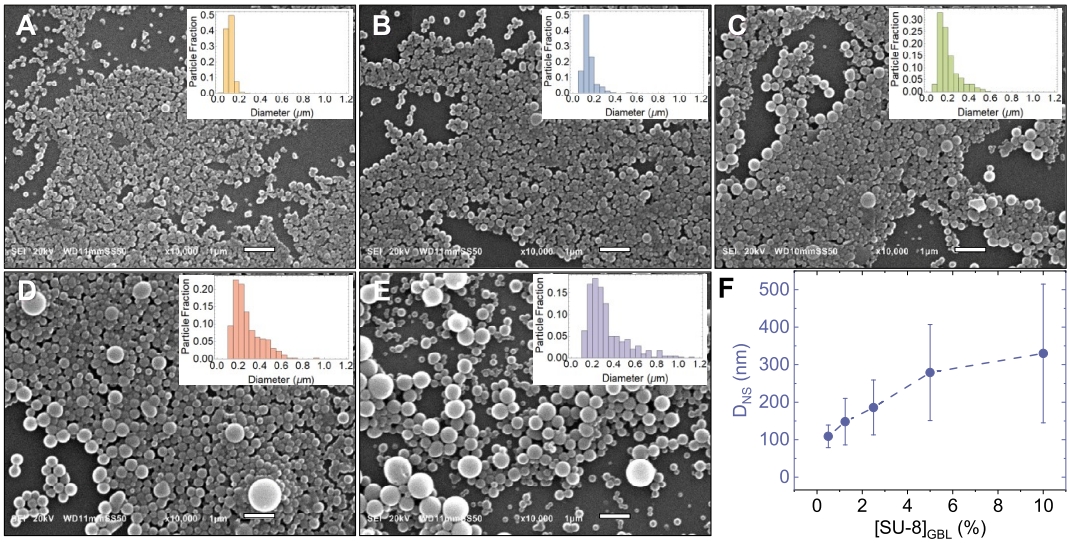

Figure 2. SEM images of the SU-8 nanospheres obtained at (A) 0.5, (B) 1.25, (C) 2.5, (D) 5, and (E) 10 wt % SU-8 polymer solutions in GBL. Insets show the size distributions of each sample. (F) Mean diameter of the SU-8 nanospheres (D_{NS}) as a function of the concentration of SU-8 in GBL. Error bars are the standard deviation of the size distributions. Scale bars are 1 μm.

nanoparticles. This immediate process stems from the rapid mixing of the organic and aqueous solvent, which leads to the instantaneous precipitation of the water-insoluble polymer and hence the formation of polymer nanoparticles in water.[16] The resulting dispersion is typically stabilized by the presence of a surfactant in the aqueous phase.

In our nanoprecipitation experiments, SU-8 is the polymer and GBL is the organic solvent. In particular, we study the effect of the SU-8 concentration, [SU-8], on the diameter of the resulting SU-8 nanospheres, as this determines the dimensions of the asperities of the resulting rough particles. Figure 2 shows SEM images of the SU-8 nanospheres obtained in water using SU-8 concentrations ranging from 0.5 to 10 wt %. From these images, we measure the diameter of the nanospheres and extract the size distributions and mean diameter (D_{NS}) at each SU-8 concentration, as shown in the insets of Figure 2A–E and the plot in Figure 2F, respectively. We observe that the mean diameter of SU-8 nanospheres increases with the increasing SU-8 concentration, from a mean diameter of 109 nm for [SU-8] = 0.5 wt % to 330 nm for [SU-8] = 10 wt %. Similar trends are reported for the nanoprecipitation in water of other hydrophobic polymers.[17,18] We note that while the size distributions are relatively narrow at low SU-8 concentrations with typical polydispersity values around 25%, they become skewed toward larger particles diameters as the SU-8 concentration increases. We attribute this effect to the coalescence of multiple nanoparticles during the nanoprecipitation at high SU-8 concentrations.[13,17,18]

Synthesis of Rough Colloidal SU-8 Rods. Next, we synthesize rough colloidal SU-8 particles by exploiting the nanoprecipitation of SU-8 in water in the presence of colloidal SU-8 particles. As shown in the schematic in Figure 3A, the coating procedure consists of two key steps. In the first step, small SU-8 nanospheres are synthesized and physisorbed onto the surface of the larger colloidal rods dispersed in the aqueous phase, presumably via van der Waals interactions. The resulting rough rods are stabilized using Pluronic F-108, a water-soluble surfactant. In the second step, the adsorbed spherical asperities are cross-linked to the surface of the rod particles via UV-light exposure, as SU-8 is a photo-sensitive material. Finally, the remaining unabsorbed SU-8 nanospheres dispersed in water are removed via centrifugation and redispersion cycles. Figure 3B–D shows SEM images of the rough rods obtained after the coating procedure. Figure 2E confirms the composite nature of the particles by labeling the spherical asperities and colloidal rods with different fluorescent dyes and imaging them with confocal microscopy.

We note that it is particularly important to ensure that the surface of the SU-8 rods is completely surfactant-free when performing the nanoprecipitation step. The presence of the surfactant on the surface of the rods dramatically reduces the physisorption of the SU-8 nanospheres onto the surface of the rods. This is demonstrated in Figure 4A, where no asperities are visible on the surface of the rods as 0.5 wt % Pluronic was present during the nanoprecipitation step. We speculate that this is due to steric repulsions mediated by the surfactant molecules which adsorb onto the surface of the rods and/or nanoprecipitated particles.[19] Finally, we also address the role of the UV-light exposure, i.e., cross-linking, on the mechanical stability of the spherical asperities adsorbed to the surface of the rods. To this end, we subjected cross-linked and uncross-linked rough rods to sonication and vortex mixing for 20 min. The SEM images shown in Figure 4B,C reveal that a significant part of the adsorbed nanospheres of the uncross-linked rough rods is lost after sonication and vortex mixing (see Figure 4B). This suggests that, despite the fact we start with cross-linked SU-8 rods,[10] these still have some residual epoxy groups on their surface, which enable their chemical bonding with the adsorbed SU-8 nanospheres upon UV-exposure. The cross-linking of the rough rods is therefore necessary to ensure proper linkage between the asperities and the rods (see Figure 4C), which is of crucial importance for applications where the particles are subjected to moderately large forces, such as in rheology experiments.

Tunability of the Asperity Size and Asperity Density. Next, we study the effect of the SU-8 concentration on the size of the asperities and asperity density on the rods. We start with an aqueous dispersion of colloidal rods with typical dimensions of 0.4 μm in diameter and 6 μm in length. To induce the nanoprecipitation of SU-8 nanospheres, we add a SU-8

https://dx.doi.org/10.1021/acs.langmuir.0c03361
Langmuir 2021, 37, 2900–2906

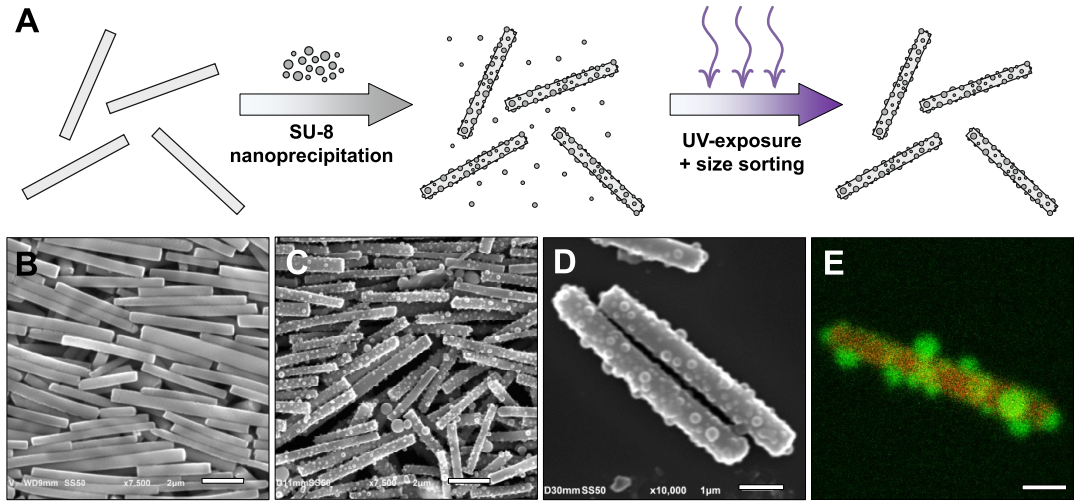

Figure 3. (A) Schematic showing the synthesis of rough colloidal SU-8 rods. In the first step, the SU-8 rods are coated with SU-8 nanoparticles formed during the nanoprecipitation of SU-8. In the second step, the adsorbed SU-8 nanospheres are cross-linked to the surface of the rods via UV-light exposure. Finally, the rough rods are separated from the unabsorbed SU-8 nanoparticles via centrifugation. SEM images of (B) the bare SU-8 rods and (C, D) rough rods. (E) Confocal microscopy image of rough SU-8 rods with the body (red) and asperities (green) labeled with two fluorescent dyes. Scale bars are 2 μm for (B, C) and 1 μm for (D, E).

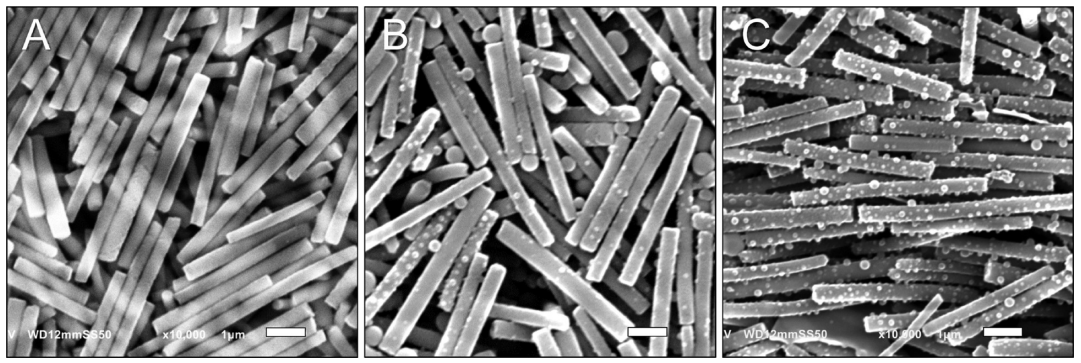

Figure 4. (A) Bare SU-8 rods obtained after the nanoprecipitation step in the presence of 0.5 wt % Pluronic in water. (B) Uncross-linked and (C) cross-linked SU-8 rough obtained after 20 min of sonication and vortex mixing. For all samples, a concentration of SU-8 of 1.25 wt % was used in the nanoprecipitation step. Scale bars are 1 μm.

solution with SU-8 concentrations ranging from 0.5 to 10 wt % as previously reported in Synthesis of SU-8 Nanospheres via Nanoprecipitation and shown in Figure 2. By analyzing SEM images as the ones shown in the insets of Figure 5, we measure both the size and the number of spherical asperities per rod at each SU-8 concentration. As shown in Figure 5G, the average asperity diameter increases with increasing SU-8 concentration, which is consistent with Figure 2, though we note that it differs from the average diameter of the nanoprecipitated spheres (see the gray line), especially at high SU-8 concentrations. This disparity is presumably due to the fact that large nanoparticles are less likely to adsorb onto the surface of the rods. We also characterize both the number density of asperities (ρ_A) and surface coverage (θ) of the rods. These two parameters are calculated as $\rho_A = N_A/A_{rod}$ and $\theta = \rho_A A_A$, where N_A is the number of asperities, A_{rod} is the average area of the cylindrical rods and A_A is the average cross-sectional area of the asperities. In our calculations, we use that $A_A = \pi(D_A/2)^2$. Note that we measure the size and number of asperities from a half of the rod surface using SEM images and assume that is the same for the other half when calculating ρ_A and θ. The plot shown in Figure 5H shows the evolution of the asperity number density and surface coverage with SU-8 concentration. Starting from bare rods, we observe that the asperity number density first increases from 4 to 20 asperities/μm^2 for 0.5 < [SU-8] < 1.25 wt % and then gradually decreases to 5 asperities/μm^2 upon increasing the concentration of SU-8. On the other hand, the surface coverage increases from 2 to 20% between SU-8 concentrations of 0.5 and 1.25 wt %, and above 1.25 wt %, the surface coverage remains roughly constant as the average asperity diameter increases with increasing [SU-8]. From both the asperity number density measurements and the SEM images shown in Figure 5A–F, we can infer that the most dense and homogeneous coating is obtained in the SU-8 concentration range of 1.25–2.5 wt %.

Finally, we discuss the separation of the rough rods from the unadsorbed SU-8 nanospheres via centrifugation. In general, it is easy to separate small spheres from larger rodlike particles via centrifugation because they sediment at different velocities.[20] However, as the diameter of the nanoprecipitated spheres increases, their separation from the rods becomes more challenging. By equating the sedimentation velocities of rods[21] and spheres, we find that D_S^*, the diameter of a sphere sedimenting at the same speed as a rod with diameter D_{rod} and length L_{rod}, is given by $D_S^* = \sqrt{\frac{3}{2}} D_{rod}\left[\ln\left(\frac{L_{rod}}{D_{rod}}\right) + c\right]^{1/2}$. Note

https://dx.doi.org/10.1021/acs.langmuir.0c03361
Langmuir 2021, 37, 2900–2906

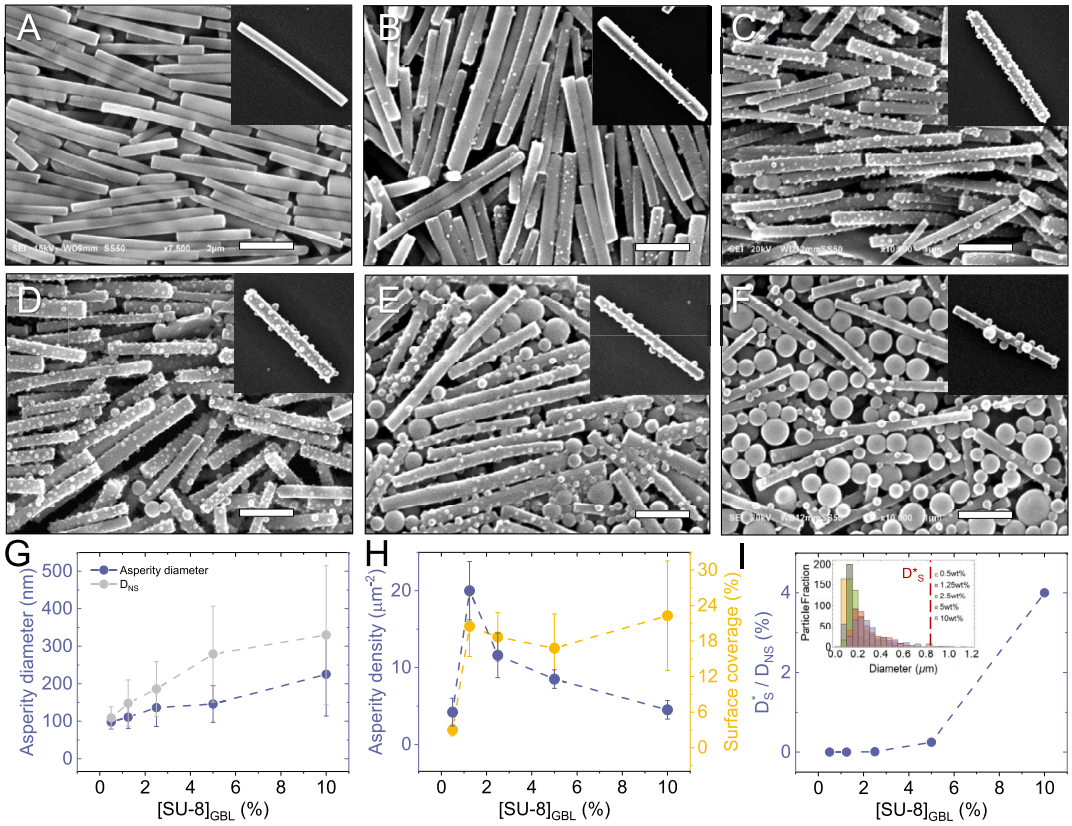

Figure 5. SEM images of rough SU-8 colloidal rods obtained at (A) 0, (B) 0.5, (C) 1.25, (D) 2.5, (E) 5, and (F) 10 wt % SU-8 in GBL. Insets show the SEM images of single rough rods. (G) Mean diameter of the asperities (blue) and SU-8 nanospheres (gray) as a function of [SU-8]. (H) Asperity number density (blue) and surface coverage (yellow) on the rods as a function of [SU-8]. (I) Percentage of SU-8 nanospheres with a diameter larger than D_S^* = 800 nm as a function of [SU-8]. Error bars are the standard deviations. Scale bars are 1 μm.

that c accounts for end effects in the sedimentation of cylindrical rods with an aspect ratio between 2 and 30.[22] In our system, we typically use rods with average dimensions of L_{rod} = 6 μm and D_{rod} = 0.4 μm, which corresponds to c = 0.312, a small value compared to that of the logarithmic term, and D_S^* = 800 nm. This suggests that unadsorbed SU-8 nanospheres with D_{NS} > 800 nm are not easily separated from the rough SU-8 rods. This is indeed confirmed by the SEM images shown in Figure 5E,F, where not only rough rods but also SU-8 nanospheres with D_{NS} > 800 nm are observed. On the other hand, Figure 5B–D show samples of mainly rough rods, consistent with the fact that the diameters of the nanoprecipitated SU-8 nanospheres for [SU-8] < 5 wt % were smaller than 800 nm (see Figure 2). In Figure 5I, we quantify this effect by showing the percentage of nanoparticles with a diameter larger than 800 nm obtained during the nanoprecipitation of SU-8 nanospheres (see Figure 2). Indeed, only for SU-8 concentrations larger than 5 wt %, there is a significant fraction of particles with a diameter larger than 800 nm, which makes their separation from the rough rods via centrifugation very cumbersome. However, an easier separation of the rough rods and the unadsorbed nanospheres obtained for [SU-8] > 5 wt % should be facilitated using rods with a larger diameter[10] or by adding salt or polymers.[23]

Beyond Colloidal Rods: Rough Colloidal SU-8 Bananas and Spheres. Recently, we developed a library of colloidal SU-8 particles with different shapes, including rods but also spheres and banana-shaped particles.[10,11] Since these particles are all made of SU-8, we can directly apply the same coating method described in Synthesis of Rough Colloidal SU-8 Rods for the colloidal SU-8 rods, to the spheres and bananas. This is indeed confirmed by the SEM images shown in Figure 6, where both rough colloidal SU-8 bananas and spheres are obtained via the nanoprecipitation of SU-8 in water. The rough bananas are particularly interesting as they provide a colloidal model system where the interplay between surface roughness phenomena and shape anisotropy can be studied as a function of the particle curvature.

Confocal Microscopy Imaging of the Concentrated Samples of Rough Colloidal SU-8 Particles. To enable the imaging of suspensions of rough colloidal SU-8 particles using confocal microscopy, we label both the asperities and the body of the colloidal SU-8 particles with a fluorescent dye. In Figure 7, we show confocal microscopy images of dense samples of rough and fluorescent SU-8 rods and bananas, where nematic ordering is observed for the rough rods (see Figure 7A) and an isotropic structure is observed for the rough bananas (see Figure 7B). The fact that they show similar phase behavior as that of the corresponding to smooth particles[10,11] illustrates the stability of our newly developed rough colloidal SU-8 particles. Also, it facilitates further studies to address the impact of surface roughness on both the structure and timescales involved in the formation of orientally ordered phases of rough particles, such as the formation of nematic glasses.[24,25]

■ CONCLUSIONS

In summary, we have successfully developed a method for the rapid fabrication of rough anisotropic colloidal SU-8 particles,

https://dx.doi.org/10.1021/acs.langmuir.0c03361
Langmuir 2021, 37, 2900−2906

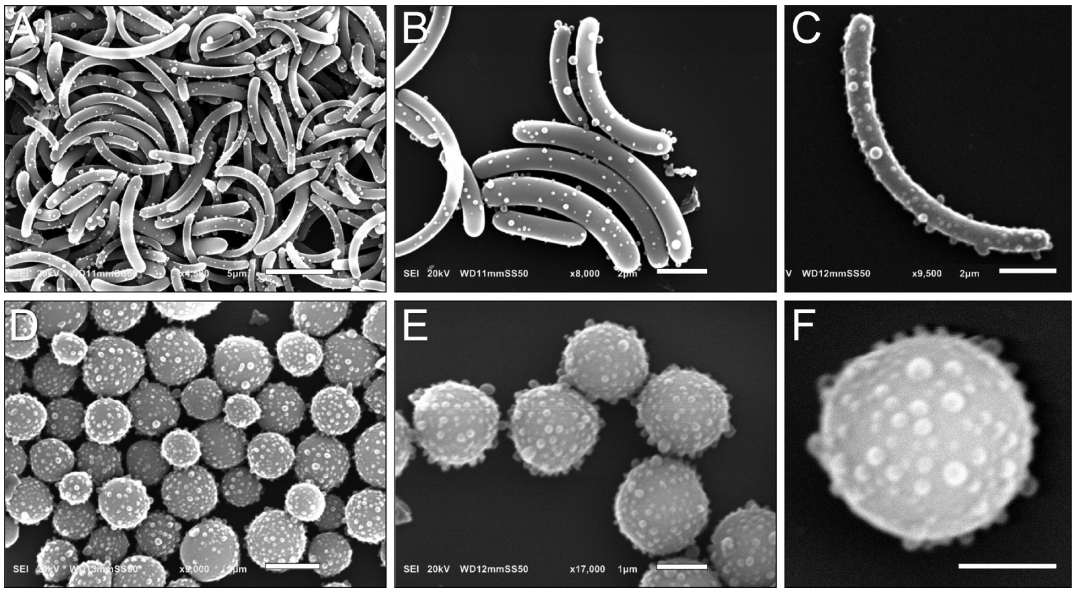

Figure 6. SEM images of rough colloidal SU-8 bananas (A–C) and spheres (D–F) obtained using 2.5 wt % [SU8]. Scale bars are 5 μm for (A), 2 μm for (B–D), and 1 μm for (E, F).

including rough colloidal rods and bananas, with tuneable asperity size and asperity density. The ease of synthesis combined with the stability and tunability of the colloidal SU-8 system[10,11] creates a range of unique possibilities to address surface roughness-related phenomena in colloidal systems of anisotropic particles. These features are particularly interesting for exploring the role of surface roughness in the rheological properties of liquid crystalline materials, which already show substantially different behavior than spherical particles due to their characteristic flow-alignment.[26] Also, the characterization

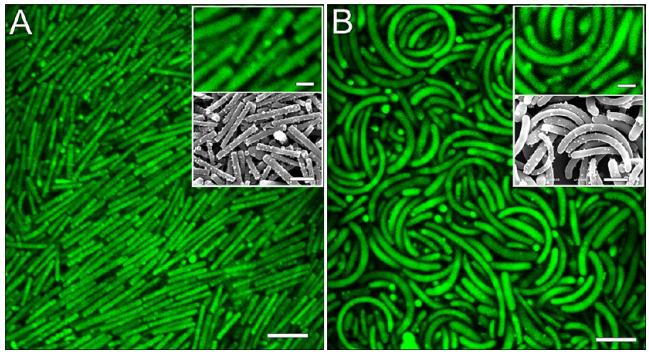

Figure 7. Confocal microscopy images of (A) a nematic phase of rough colloidal SU-8 rods and (B) a dense isotropic phase of rough bananas. The insets show a zoom of the confocal image and the SEM images of the corresponding particles, where their surface roughness can be clearly observed. Scale bars are 5 μm for the main panels and 1 μm for the insets.

of the structure and dynamics of these "rough" liquid crystalline phases might lead to a deeper understanding of the formation of nematic glasses.[24,25] Moreover, direct imaging of the suspensions of fluorescently labeled rough particles under shear could be used to elucidate the role of interparticle friction during shear thickening, which for rods is observed at much lower volume fractions than for spheres,[27] and is associated with complex fluctuations in orientational order.[28] Controlling the surface roughness of the colloidal SU-8 rods could also be used to study the effect of roughness on the depletion-driven formation of nematic tactoids[29] and on their performance as foam stabilizers,[30] where anisotropic particles have already shown outstanding stability efficiencies.[30,31] Finally, the rough colloidal bananas promise an even richer behavior as they will allow addressing the effect of particle curvature on the rheological, wetting or the self-assembly properties of rough anisotropic particles.

AUTHOR INFORMATION

Corresponding Authors

Carla Fernández-Rico – *Department of Chemistry, Physical and Theoretical Chemistry Laboratory, University of Oxford, Oxford OX1 3QZ, United Kingdom*; orcid.org/0000-0002-9472-1073; Email: carla.fernandezrico@chem.ox.ac.uk

Roel P. A. Dullens – *Department of Chemistry, Physical and Theoretical Chemistry Laboratory, University of Oxford, Oxford OX1 3QZ, United Kingdom*; Email: roel.dullens@chem.ox.ac.uk

Author

Jeffrey S. Urbach – *Department of Physics and Institute for Soft Matter Synthesis and Metrology, Georgetown University, Washington, District of Columbia 20057, United States*

Complete contact information is available at: https://pubs.acs.org/10.1021/acs.langmuir.0c03361

Notes

The authors declare no competing financial interest.

ACKNOWLEDGMENTS

We thank the ERC (ERC Consolidator Grant No. 724834 – OMCIDC) is acknowledged for financial support.

REFERENCES

(1) Hu, M.; Hsu, C. P.; Isa, L. Particle Surface Roughness as a Design Tool for Colloidal Systems. *Langmuir* **2020**, *36*, 11171–11182.

(2) Lootens, D.; Van Damme, H.; Hémar, Y.; Hébraud, P. Dilatant flow of concentrated suspensions of rough particles. *Phys. Rev. Lett.* **2005**, *95*, No. 268302.
(3) Hsu, C.-P.; Ramakrishna, S. N.; Zanini, M.; Spencer, N. D.; Isa, L. Roughness-dependent tribology effects on discontinuous shear thickening. *Proc. Natl. Acad. Sci. U.S.A.* **2018**, *115*, 5117−5122.
(4) Petel, O. E.; Higgins, A. J. Shock wave propagation in dense particle suspensions. *J. Appl. Phys.* **2010**, *108*, No. 114918.
(5) Zanini, M.; Marschelke, C.; Anachkov, S. E.; Marini, E.; Synytska, A.; Isa, L. Universal emulsion stabilization from the arrested adsorption of rough particles at liquid-liquid interfaces. *Nat. Commun.* **2017**, *8*, No. 15701.
(6) San-Miguel, A.; Behrens, S. H. Influence of nanoscale particle roughness on the stability of pickering emulsions. *Langmuir* **2012**, *28*, 12038−12043.
(7) Kraft, D. J.; Ni, R.; Smallenburg, F.; Hermes, M.; Yoon, K.; Weitz, D. A.; Van Blaaderen, A.; Groenewold, J.; Dijkstra, M.; Kegel, W. K. Surface roughness directed self-assembly of patchy particles into colloidal micelles. *Proc. Natl. Acad. Sci. U.S.A.* **2012**, *109*, 10787−10792.
(8) Kamp, M.; Hermes, M.; Van Kats, C. M.; Kraft, D. J.; Kegel, W. K.; Dijkstra, M.; Van Blaaderen, A. Selective Depletion Interactions in Mixtures of Rough and Smooth Silica Spheres. *Langmuir* **2016**, *32*, 1233−1240.
(9) Zanini, M.; Hsu, C. P.; Magrini, T.; Marini, E.; Isa, L. Fabrication of rough colloids by heteroaggregation. *Colloids Surf., A* **2017**, *532*, 116−124.
(10) Fernández-Rico, C.; Yanagishima, T.; Curran, A.; Aarts, D. G. A. L.; Dullens, R. P. A. Synthesis of Colloidal SU-8 Polymer Rods Using Sonication. *Adv. Mater.* **2019**, *31*, No. 1807514.
(11) Fernández-Rico, C.; Chiappini, M.; Yanagishima, T.; de Sousa, H.; Aarts, D. G. A. L.; Dijkstra, M.; Dullens, R. P. A. Shaping colloidal bananas to reveal biaxial, splay-bend nematic, and smectic phases. *Science* **2020**, *369*, 950−955.
(12) Fessi, H.; Puisieux, F.; Devissaguet, J. P.; Ammoury, N.; Benita, S. Nanocapsule formation by interfacial polymer deposition following solvent displacement. *Int. J. Pharm.* **1989**, *55*, R1−R4.
(13) Hornig, S.; Heinze, T.; Becer, C. R.; Schubert, U. S. Synthetic polymeric nanoparticles by nanoprecipitation. *J. Mater. Chem.* **2009**, *19*, 3838−3840.
(14) Wang, Y.; Li, P.; Tran, T. T. D.; Zhang, J.; Kong, L. Manufacturing techniques and surface engineering of polymer based nanoparticles for targeted drug delivery to cancer. *Nanomaterials* **2016**, *6*, No. 26.
(15) Tao, J.; Chow, S. F.; Zheng, Y. Application of flash nanoprecipitation to fabricate poorly water-soluble drug nanoparticles. *Acta Pharm. Sin. B* **2019**, *9*, 4−18.
(16) Zhao, C.; Melis, S.; Hughes, E. P.; Li, T.; Zhang, X.; Olmsted, P. D.; Van Keuren, E. Particle Formation Mechanisms in the Nanoprecipitation of Polystyrene. *Langmuir* **2020**, *36*, 13210−13217.
(17) Beck-Broichsitter, M.; Rytting, E.; Lebhardt, T.; Wang, X.; Kissel, T. Preparation of nanoparticles by solvent displacement for drug delivery: A shift in the " ouzo region" upon drug loading. *Eur. J. Pharm. Sci.* **2010**, *41*, 244−253.
(18) Galindo-Rodriguez, S.; Allémann, E.; Fessi, H.; Doelker, E. Physicochemical parameters associated with nanoparticle formation in the salting-out, emulsification-diffusion, and nanoprecipitation methods. *Pharm. Res.* **2004**, *21*, 1428−1439.
(19) Opdam, J.; Tuinier, R.; Hueckel, T.; Snoeren, T. J.; Sacanna, S. Selective colloidal bonds via polymer-mediated interactions. *Soft Matter* **2020**, *16*, 7438−7446.
(20) Sharma, V.; Park, K.; Srinivasarao, M. Shape separation of gold nanorods using centrifugation. *Proc. Natl. Acad. Sci. U.S.A.* **2009**, *106*, 4981−4985.
(21) Beoeesma, S. Viscous force constant for a closed cylinder. *J. Chem. Phys.* **1960**, *32*, 1632−1635.
(22) Tirado, M. M.; Martínez, C. L.; de La Torre, J. G. Comparison of theories for the translational and rotational diffusion coefficients of rod-like macromolecules. Application to short DNA fragments. *J. Chem. Phys.* **1984**, *81*, 2047−2052.
(23) Gui, H.; Chen, H.; Khripin, C. Y.; Liu, B.; Fagan, J. A.; Zhou, C.; Zheng, M. A facile and low-cost length sorting of single-wall carbon nanotubes by precipitation and applications for thin-film transistors. *Nanoscale* **2016**, *8*, 3467−3473.
(24) Solomon, M. J.; Spicer, P. T. Microstructural regimes of colloidal rod suspensions, gels, and glasses. *Soft Matter* **2010**, *6*, 1391−1400.
(25) Dhont, J. K. G.; Kang, K.; Kriegs, H.; Danko, O.; Marakis, J.; Vlassopoulos, D. Nonuniform flow in soft glasses of colloidal rods. *Phys. Rev. Fluids* **2017**, *2*, No. 043301.
(26) Xu, Y.; Atrens, A.; Stokes, J. R. A review of nanocrystalline cellulose suspensions: Rheology, liquid crystal ordering and colloidal phase behaviour. *Adv. Colloid Interface Sci.* **2020**, *275*, No. 102076.
(27) James, N. M.; Xue, H.; Goyal, M.; Jaeger, H. M. Controlling shear jamming in dense suspensions: Via the particle aspect ratio. *Soft Matter* **2019**, *15*, 3649−3654.
(28) Rathee, V.; Arora, S.; Blair, D. L.; Urbach, J. S.; Sood, A. K.; Ganapathy, R. Role of particle orientational order during shear thickening in suspensions of colloidal rods. *Phys. Rev. E* **2020**, *101*, No. 040601(R).
(29) Modlinska, A.; Alsayed, A. M.; Gibaud, T. Condensation and dissolution of nematic droplets in dispersions of colloidal rods with thermo-sensitive depletants. *Sci. Rep.* **2015**, *5*, No. 18432.
(30) Alargova, R. G.; Warhadpande, D. S.; Paunov, V. N.; Velev, O. D. Foam superstabilization by polymer microrods. *Langmuir* **2004**, *20*, 10371−10374.
(31) Madivala, B.; Vandebril, S.; Fransaer, J.; Vermant, J. Exploiting particle shape in solid stabilized emulsions. *Soft Matter* **2009**, *5*, 1717−1727.

https://dx.doi.org/10.1021/acs.langmuir.0c03361
Langmuir 2021, 37, 2900−2906